

Self-limited nanosecond laser-induced bubble growth in sealed containers

Cite as: Appl. Phys. Lett. **119**, 064101 (2021); doi: [10.1063/5.0063048](https://doi.org/10.1063/5.0063048)

Submitted: 11 July 2021 · Accepted: 3 August 2021 ·

Published Online: 11 August 2021





View Online



Export Citation



CrossMark

Hamid Ebrahimi Orimi,^{1,2} Leonardo Arreaza,¹ Sivakumar Narayanswamy,²  and Christos Boutopoulos^{1,3,4,a)} 

AFFILIATIONS

¹Centre de Recherche Hôpital Maisonneuve-Rosemont, Montréal, Quebec HIT 2M4, Canada

²Department of Mechanical, Industrial and Aerospace Engineering, Concordia University, Montréal, Quebec H3G 1M8, Canada

³Department of Ophthalmology, Faculty of Medicine, University of Montreal, Montréal, Quebec H3C 3J7, Canada

⁴Institute of Biomedical Engineering, University of Montreal, Montreal, Quebec H3C 3J7, Canada

^{a)}Author to whom correspondence should be addressed: christos.boutopoulos@umontreal.ca

ABSTRACT

We demonstrate that nanosecond laser-induced bubbles, generated in sealed containers, can experience self-limiting effects. We experimentally study such effects using simultaneous pressure and bubble dynamics recordings. We show that self-limiting effects can be drastic for mm-sized bubbles generated in sub-cm³ sized containers, resulting in 0.5-fold decrease in their size and fourfold decrease in their lifetime compared to those generated in non-sealed control containers. We use the Keller–Miksis equation to model self-limiting effects and discuss their technological implications in applications that exploit bubble growth in confined geometries.

Published under an exclusive license by AIP Publishing. <https://doi.org/10.1063/5.0063048>

Laser-induced cavitation bubbles are central in a variety of biomedical applications, including eye surgery,¹ high-speed cell sorting,² needle-free injection,³ bioprinting,⁴ and laser lithotripsy.⁵ In most of the cavitation bubble-enabled applications, bubble growth is confined or semi-confined in a liquid container. Understanding of how confined geometries affect bubble dynamics (i.e., their size and lifetime) is essential to optimize existing applications and to eventually engineer future applications that can benefit from bubble confinement effects.

Significant efforts have been made toward understanding bubble growth near rigid^{6,7} and elastic^{8,9} boundaries, or between them.¹⁰ Limiting bubbles with such boundaries significantly reduces their size and lifetime due to local liquid compressibility.^{11,12} Previous studies have also shown that varying the externally applied pressure to a sealed container can drastically affect bubble dynamics.^{13,14} For example, laser-induced bubbles in a 3 MPa pressurized chamber have ~30-times smaller volume and ~17-times shorter lifetime compared to those generated in a non-pressurized chamber using identical laser conditions.¹⁴

Historically, fundamental studies on laser-induced bubble dynamics have been conducted in large containers, where self-limiting effects are negligible (i.e., external pressure is 1 atm). Interestingly, bubble confinement effects were both experimentally and theoretically observed in ballistic penetration of reservoirs filled with a liquid, where the generation of highly energetic bubbles is common.¹⁵ The work

described in here is motivated by the absence of studies reporting self-limiting effects in laser-induced bubbles and by the importance of those effects in virtually any application that exploits bubbles generation in confined or semi-confined reservoirs, such as microfluidic chambers and microcapillaries. Here, we sought to address such self-limiting effects and designed an experimental setting to reveal them.

In this Letter, we show that self-limiting effects appear when laser-induced mm-sized bubbles are generated in small sealed containers. We investigate the self-limiting effect using simultaneous bubble dynamics and liquid pressure recordings. We show that pressure waves generated by the bubble expansion can in turn modulate bubble growth (i.e., self-limiting effect), resulting in drastic spatiotemporal bubble confinement. Finally, we use Keller–Miksis modeling to explain self-limiting effects and discuss their technological implications.

We generated cavitation bubbles using nanosecond (ns) laser pulses (Nano L series, Litron Lasers, 6 ns, 532 nm). We used microcentrifuge tubes with built-in optical windows (glass cover slips) as sealed containers (Fig. 1). We filled the containers with thoroughly degassed distilled water and hermetically sealed them using a protocol provided in the [supplementary material](#). The laser beam was expanded to ~12 mm in diameter and focused at the center of the containers using a 4X objective lens (PLN4X, NA = 0.1, Olympus). We used two measuring systems to simultaneously monitor bubble dynamics and pressure increase inside the container. Briefly, we used a continuous wave

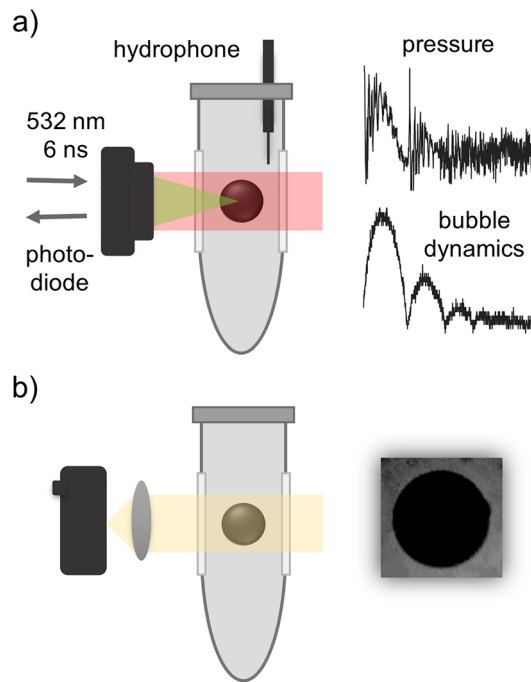


FIG. 1. Schematic overview of the experimental setup used to study self-limited bubble growth in sealed containers. (a) Simultaneous measurement of bubble dynamics and liquid pressure, and (b) measurement of bubble maximum radius.

laser beam (633 nm) to measure bubble dynamics and a hydrophone (rise time: 50 ns) (Müller-Platte Needle Probe, Müller Instruments), placed inside the sealed container, to record liquid pressure [Fig. 1(a)]. Finally, images of bubbles were taken using a high-speed camera (Chronos 1.4, Kron Technologies) [Fig. 1(b)]. We used a beam sampling approach to measure the laser energy. We recorded the energy of each laser pulse using a pyroelectric sensor (QE12LP-S-MB, Gentec Electro-Optics). Then, we used the transmission coefficient of the setup to deduce the energy at the sample level, which is the reported value throughout the study. A detailed schematic of the experimental setup is presented in Fig. S1.

With previous theoretical work, we have shown that laser-induced bubbles experience self-limited growth in confined geometries due to water compressibility.³ Here, we sought to experimentally investigate this “damping” effect and its dependence on key experimental settings, such as the container volume and laser energy. We used three sealed containers, namely, 0.3, 0.6, and 1.9 ml, and varied the laser pulse energy from 1.5 to 3.25 mJ. Note that we determined the cavitation threshold (80% cavitation probability) for our irradiation setting to be $E_{th} = 1.25$ mJ [see Fig. S2(a)]. We also used a large (50 ml) non-sealed container to perform control experiments.

Figure 2(a) shows the results of an indicative series of experiments, where bubbles were generated at 1.75 mJ in different containers. We found that bubbles in sealed containers had much shorter lifetime (53 μ s for 0.3 ml, 79 μ s for 0.6 ml, and 111 μ s for 1.9 ml) compared to those generated in an open control container (123 μ s). Furthermore, bubbles generated in sealed containers had smaller size (535 μ m for 0.3 ml, 572 μ m for 0.6 ml, and 627 μ m for 1.9 ml)

compared to those generated in an open container (731 μ m). These results reveal a predominant self-limiting effect in bubble growth that strongly depends on the volume of the sealed container, V_c . We systematically studied this effect as a function of the laser energy [Fig. 2(b)], E_l . For $E_l \geq 2 \cdot E_{th}$ and open control container, we found that $R_{max} \sim E_l^{0.32}$, which is consistent with the extended literature in large containers^{16,17} and reflects the energy balance when liquid pressure is equal to 1 atm. However, this relation changes for sealed containers in a volume-dependent manner: $R_{max} \sim E_l^{0.26}$ for $V_c = 1.9$ ml, $R_{max} \sim E_l^{0.19}$ for $V_c = 0.6$ ml, and $R_{max} \sim E_l^{0.25}$ for $V_{cr} = 0.3$ ml. We will show later that lower exponent values for sealed containers compared to the open container do not represent bubbles of lower energy. We found a similar effect for the bubble lifetime, t_{BLF} : $t_{BLF} \sim E_l^{0.39}$ for the open control container, $t_{BLF} \sim E_l^{0.455}$ for $V_c = 1.9$ ml, $t_{BLF} \sim E_l^{0.044}$ for $V_c = 0.6$ ml, and $t_{BLF} \sim E_l^{0.0001}$ for $V_c = 0.3$ ml [Fig. 2(c)]. There are two important practical implications of those findings: (i) for a given laser energy, the maximum bubble size depends on the volume of the sealed container and (ii) the bubble lifetime is virtually independent of the laser energy for small sealed containers.

The liquid pressure inside the container, P_l , is a key factor affecting bubble dynamics. Therefore, we sought to measure the time-dependent P_l for both open and sealed containers. Figure 3(a) presents P_l along with the corresponding bubble temporal profile in both sealed and open containers for $E_l = 2.5$ mJ. We found only marginal P_l variations for the open container, indicating that bubble growth is not affected by the container itself. For all sealed containers, we found significant P_l modulation that is strongly correlated with the bubble dynamics. First, there is an increase in P_l up to a maximum value, corresponding to the bubble growth phase. Note that the time point of maximum bubble size coincides with that of maximum P_l for all sealed containers. Next, P_l decreases due to bubble contraction and reaches a minimum value at bubble collapse. We filtered the raw hydrophone data to remove shock-wave generation, shockwave reflections, and noise components. Using the filtered signal [red line in Fig. 3(a)], we calculated the maximum increase in P_l as a function of the laser energy for all containers. P_l increase was marginal and independent of E_l for the controlled container. However, we found a strong correlation between the laser energy and maximum P_l for all sealed containers [Fig. 3(b)]. Overall, these results indicate that bubble growth in sealed containers results in the generation of a pressure wave due to liquid compression. Both the laser energy and the sealed container volume affect the amplitude of the pressure wave, while its temporal profile follows the bubble dynamics. For the examined settings, we found that the maximum amplitude of the liquid pressure wave was 3.8 bar (sealed 0.3 ml), which is one order of magnitude smaller compared to that of a decaying shock wave released upon bubble generation and collapse.¹⁸ The life span of the generated pressure waves (~ 55 to 160 μ s) is two orders of magnitude larger compared to the of the corresponding shock wave.

To examine whether the laser to bubble energy conversion efficiency is maintained in the different settings, we used the following equation to calculate the bubble energy for sealed and controlled containers:

$$E_b = \frac{4}{3} \pi (P_l - P_v) R_{max}^3, \quad (1)$$

where P_l is the liquid pressure far from the bubble when it reaches its maximum radius, P_v is the saturated vapor pressure in the bubble, and

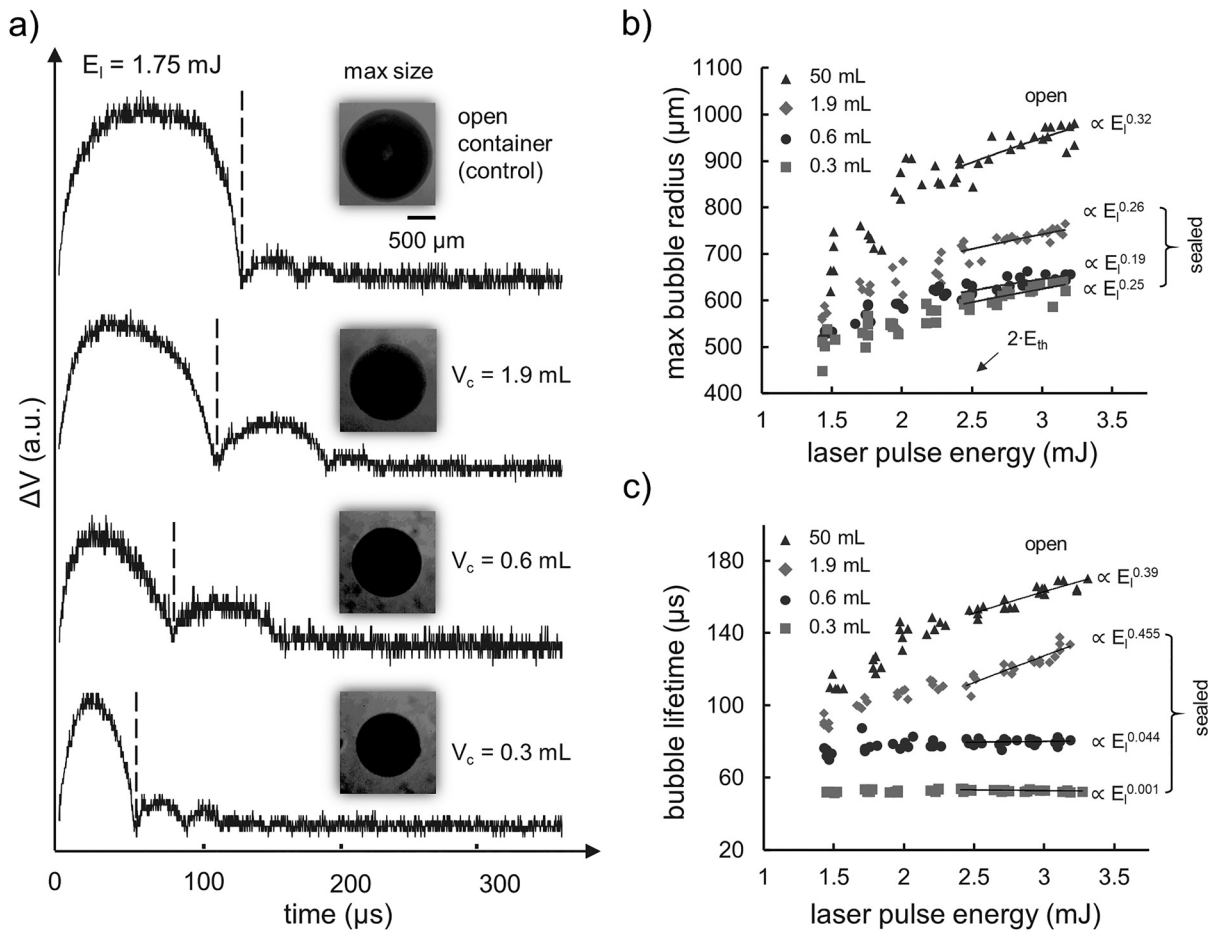


FIG. 2. Self-limited bubble growth in sealed containers. (a) Indicative bubble dynamics traces (i.e., inverted photodiode signal) and bubble images for sealed containers (0.3 ml, 0.6 and 1.9 ml) and an open control container (15 ml). Bubbles were generated at 1.75 mJ, and images were acquired using sufficiently long integration time (100 μs) to depict max bubble size. The dependence of the maximum bubble radius (b) and bubble lifetime (c) on the laser energy for sealed and control containers. The dependence on the laser energy is fitted for $E_l \geq 2 \cdot E_{th}$.

R_{max} is the maximum bubble radius. Using the maximum P_1 [Fig. 3(b)] and maximum bubble radius [Fig. 2(b)], we found that the laser to bubble energy conversion efficiency (E_{bubble}/E_{pulse}) is relatively constant ($\sim 12\%$ for $E_l \geq 2 \cdot E_{th}$) independently of the container volume and configuration (i.e., open/sealed) [Fig. S2(b)].

Next, we sought to validate whether the implementation of experimentally measured P_1 in a bubble model would allow modeling of the confinement effect. To do so, we used the Keller-Miksis (KM) equation

$$\left(1 - \frac{\dot{R}}{c}\right) R \ddot{R} + \frac{3}{2} \dot{R}^2 \left(1 - \frac{\dot{R}}{3c}\right) = \frac{1}{\rho} \left(1 + \frac{\dot{R}}{c}\right) \left[\left(P_g - P_v + \frac{2\sigma_1}{R_0}\right) \left(\frac{R_0}{R}\right)^{3\gamma} + P_v - P_l \right] - 4\nu \frac{\dot{R}}{R} - \frac{2\sigma_1}{\rho R} - \frac{3}{c\rho} \left(P_g - P_v + \frac{2\sigma_1}{R_0}\right) \left(\frac{R_0}{R}\right)^{3\gamma} \dot{R}, \quad (2)$$

where c is the speed of sound in the liquid, ρ is the liquid density, γ is the heat capacity ratio, R is the bubble radius, R_0 is the bubble initial

radius ($t=0$), ν is the kinematic viscosity, σ_1 is the surface tension, and P_g is the initial gas pressure in the bubble ($t=0$). Our modeling approach consists of two steps: First, for a given laser energy, we determined a set of initial conditions (R_0 , P_g). We have previously reported in detail our approach to determine the initial conditions.³ We present in the [supplementary material](#) the adaptation of this approach for the KM model. For a given energy, initial conditions were considered independent of both the container volume and configuration (i.e., open/sealed). Next, for a given laser energy and container configuration, we used the experimentally measured P_1 profile [Fig. 3(a)] to calculate bubble growth. All modeling parameters can be found in the [supplementary material](#) (Table S1 and Table S2).

Figure 4 summarizes our modeling results on the self-limited bubble growth. In accordance with the experimental results, the KM model shows that both R_{max} and bubble lifetime are suppressed in sealed containers due to an increase in P_1 (Fig. 4). For R_{max} , there is a very good agreement between the KM model and experiments for the entire spectrum of tested settings [Fig. 4(b)]. This reflects the

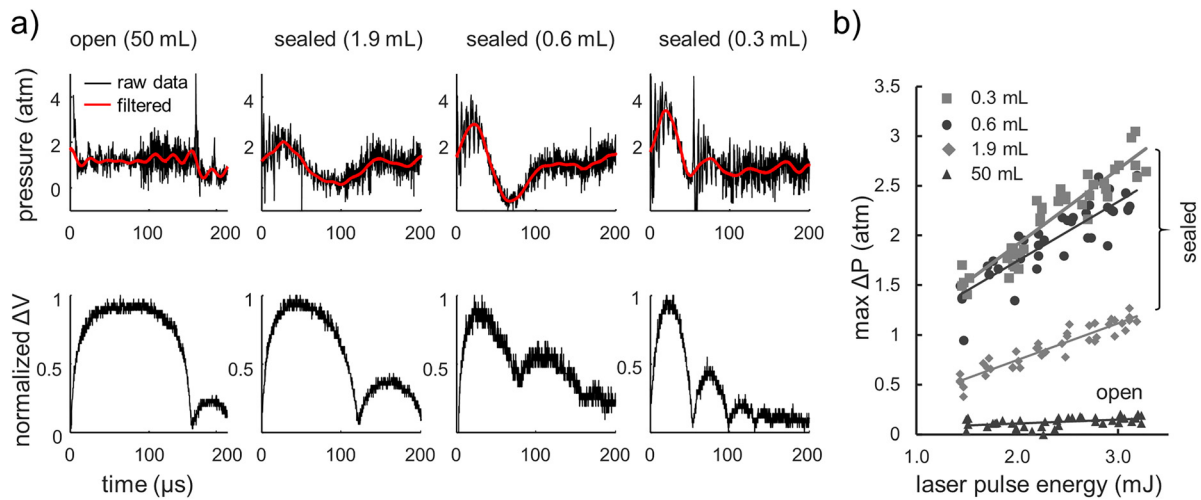


FIG. 3. Pressure profiles for sealed and control containers. (a) Indicative ($E_l = 2.5$ mJ) liquid pressure recordings (top) and corresponding bubble dynamics traces (bottom) (i.e., inverted photodiode signal) for sealed containers (0.3, 0.6, and 1.9 ml) and an open control container (15 ml). The raw data were filtered to remove the high frequency component (noise and/or shockwaves). (b) The dependence of the maximum pressure variance on the laser energy for sealed and control containers.

preservation of the laser to bubble energy conversion efficiency [Fig. S2(b)]. Although the KM model shows temporal confinement of the bubble as well [Fig. 4(a)], there is a systematic overestimation of the bubble maximum size time point. Note that we compare this time point instead of the bubble lifetime [Fig. 4(b)], since bubble collapse did not occur for several experimental settings due to the pressure wave [i.e., $V_c = 0.6$ ml in Fig. 4(a)], an effect we also experimentally observed [Fig. 3(a), $V_c = 0.6$ ml]. Differences between the modeled and experimental temporal profiles can be attributed to the limitations of our experimental setting. In fact, P_1 is being measured far from the bubble; thus, the model underestimates the actual pressure experienced by the bubble wall during the expansion phase. Note that the KM model assumes spherical bubbles. In our experimental setting, fast

bubble imaging showed that this condition is met during the bubble growth phase. However, there is a loss of spherical symmetry in the late stage of the bubble collapse phase, which also limits the accuracy of our model.

In conclusion, we showed that laser-induced bubble growth in sealed containers can be spatiotemporally self-limited. Using both experimental measurements and modeling, we attributed the self-limiting effect to the generation of a pressure wave, whose amplitude and lifespan depend on the laser energy and the volume of the container. Interestingly, the self-limiting effect is predominant on the bubble lifetime, which becomes virtually independent of the laser energy for small sealed containers. We also found that the laser to bubble energy conversion efficiency is preserved in self-limited bubbles.

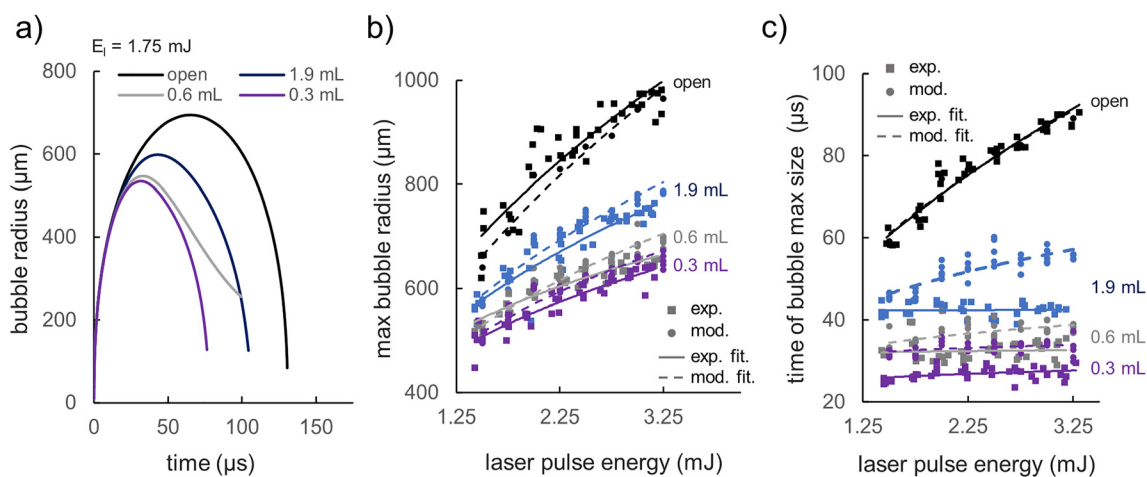


FIG. 4. Keller-Miksis bubble modeling using the experimentally measured pressure profiles. (a) KM bubble modeling for sealed containers (0.3, 0.6, and 1.9 ml) and an open control container (15 ml). $E_l = 1.5$ mJ. The dependence of the experimentally measured and modeled bubble behavior on the laser energy for open and sealed containers: (b) maximum bubble size, (c) time of bubble maximum size.

Technological implications of these findings are important for designing devices that exploit bubble growth in small volume containers, such as laser-actuated microfluidics and laser-induced microjet devices.

See the [supplementary material](#) for details on the experimental setup, sample preparation, cavitation threshold, and energy balance determination as well as additional information on the modeling approach.

The authors acknowledge Natural Sciences and Engineering Research Council of Canada (No. RGPIN-2018-06767; C.B.) and Fonds de Recherche du Québec–Nature et technologies (Ph.D. scholarship; H.E.O.). C.B. is the recipient of a Junior I salary award from Fonds de la Recherche en Santé du Québec (FRSQ) (Nos. 253123 and 265459).

DATA AVAILABILITY

The data that support the findings of this study are available from the corresponding author upon reasonable request.

REFERENCES

- ¹E. A. Brujan and A. Vogel, *J. Fluid Mech.* **558**, 281 (2006).
- ²T. H. Wu, Y. Chen, S. Y. Park, J. Hong, T. Teslaa, J. F. Zhong, D. D. Carlo, M. A. Teitell, and P. Y. Chiou, *Lab Chip* **12**, 1378 (2012).
- ³H. E. Orimi, S. Narayanswamy, and C. Boutopoulos, *J. Fluids Struct.* **98**, 103079 (2020).
- ⁴H. E. Orimi, S. S. Hosseini Kolkoo, E. Hooker, S. Narayanswamy, B. Larrivée, and C. Boutopoulos, *Sci. Rep.* **10**, 9730 (2020).
- ⁵K. Rink, G. Delacrétaz, and R. P. Salathé, *Appl. Phys. Lett.* **61**, 258 (1992).
- ⁶T. Požar, V. Agrež, and R. Petkovšek, *Ultrason. Sonochem.* **73**, 105456 (2021).
- ⁷D. Horvat, U. Orthaber, J. Schille, L. Hartwig, U. Löschner, A. Vrečko, and R. Petkovšek, *Int. J. Multiphase Flow* **100**, 119 (2018).
- ⁸B. Dollet, P. Marmottant, V. Garbin, B. Dollet, P. Marmottant, V. Garbin, B. Dynamics, B. Dollet, P. Marmottant, and V. Garbin, *Annu. Rev. Fluid Mech.* **51**, 331 (2019).
- ⁹E. A. Brujan, K. Nahen, P. Schmidt, and A. Vogel, *J. Fluid Mech.* **433**, 251 (2001).
- ¹⁰E. A. Brujan, T. Noda, A. Ishigami, T. Ogasawara, and H. Takahira, *J. Fluid Mech.* **841**, 28 (2018).
- ¹¹C. Lechner, M. Koch, W. Lauterborn, and R. Mettin, *J. Acoust. Soc. Am.* **142**, 3649 (2017).
- ¹²W. Lauterborn, C. Lechner, M. Koch, and R. Mettin, *IMA J. Appl. Math.* **83**, 566 (2018).
- ¹³B. B. Li, H. C. Zhang, J. Lu, and X. W. Ni, *Opt. Laser Technol.* **43**, 1499 (2011).
- ¹⁴K. Sasaki, T. Nakano, W. Soliman, and N. Takada, *Appl. Phys. Express* **2**, 046501 (2009).
- ¹⁵T. Fourest, J. M. Laurens, E. Deletombe, J. Dupas, and M. Arrigoni, *Thin-Walled Struct.* **86**, 67 (2015).
- ¹⁶R. Petkovšek and P. Gregorčič, *J. Appl. Phys.* **102**, 044909 (2007).
- ¹⁷A. Vogel, J. Noack, K. Nahen, D. Theisen, S. Busch, U. Parlitz, D. X. Hammer, G. D. Noojin, B. A. Rockwell, and R. Birngruber, *Appl. Phys. B* **68**, 271 (1999).
- ¹⁸A. Vogel, S. Busch, and U. Parlitz, *J. Acoust. Soc. Am.* **100**, 148 (1996).